



# The analytical beam element model: novel approach for fast calculation of vibrations in electric machines

Martin Enno Gerlach · Allan de Barros · Xudong Huang · Markus Langfermann · Bernd Ponick · Amir Ebrahimi

Received: 25 November 2022 / Accepted: 30 January 2023 / Published online: 16 March 2023  
 © The Author(s) 2023, corrected publication 2023

**Abstract** The vibration and acoustic behavior of electric machines is an important aspect of the design process. A crucial part of the modeling is the correct prediction of the stator's vibration behavior, characterized by the stator's eigenfrequencies and eigenmodes. For this purpose, a calculation approach called the analytical beam element model (ABM) was presented in a previous paper [18], where *Euler–Bernoulli* beams were used to describe the vibration behavior of the stator. The ABM introduced offers an alternative to the finite element (FE) method and to classical analytical models. In this paper, the model is examined and extended further. Different approaches conceived to better describe the influence of the stator yoke's thickness by using Timoshenko beams and a multi-layer discretization are presented and discussed. Furthermore, a new feature that considers the lever arm effect of the stator teeth with respect to the yoke is introduced. The results are compared to FE calculations and measurements. Lastly, the improved ABM is used to calculate the vibration behavior of four stators with outer diameters ranging from 160 mm to 7 m. The results are compared to FE results to prove the accuracy of the ABM.

**Keywords** Electric machines · Finite element analysis · Magnetic cores · Numerical models ·

Stators · Vibrations · Eigenfrequencies · Eigenmodes · Analytical calculation · Beam element

## Das Analytische Balkenelement-Modell: ein neuer Ansatz zur Berechnung des Schwingungsverhaltens elektrischer Maschinen

**Zusammenfassung** Die Berechnung des Schwingungsverhaltens elektrischer Maschinen ist ein wichtiger Bestandteil bei der Dimensionierung elektrischer Maschinen. Die schnelle und genaue Berechnung des mechanischen Schwingungsverhaltens, das durch die Eigenfrequenzen und -formen des Ständers bestimmt wird, stellt dabei eine Herausforderung dar. In dieser Arbeit wird ein neuer Berechnungsansatz vorgestellt, der auf einem analytischen Balkenelement beruht, und eine Alternative zu der Finite-Elemente-Methode (FEM) und den konventionellen analytischen Berechnungsansätzen ist. Das Analytische Balkenelement-Modell (ABM) wurde bereits in [18] eingeführt und anhand einer Beispielmachine validiert. In dieser Arbeit wird das ABM weiter untersucht, erweitert und modifiziert. Der Einfluss der Ständerjochhöhe auf die Eigenfrequenzen und -formen wird modelliert. Dafür werden zwei unterschiedliche Balkenelement-Modelle, der *Euler–Bernoulli*-Balken und der *Timoshenko*-Balken, verwendet, und der Ständer wird mit mehreren Lagen von Balkenelementen modelliert. Zusätzlich wird die Verbindung der Zähne zum Ständerjoch untersucht. Eine Koordinatentransformation wird verwendet, um die Hebelwirkung der Ständerzähne auf das Ständerjoch zu berücksichtigen. Das modifizierte ABM wird anhand von Messungen und FE-Berechnungen der Beispielmachine aus [18] validiert. Darüber hinaus wird das ABM verwendet, um das Schwingungsverhalten von vier unterschiedlichen Statoren mit Außendurchmessern von 160 mm bis 7 m zu bestimmen. Die Ergebnisse werden mit FE-Berech-

This work was supported by the German Federal Ministry of Economic Affairs and Energy on the basis of a decision by the German Bundestag.

M. E. Gerlach (✉) · A. de Barros · X. Huang ·  
 M. Langfermann · B. Ponick · A. Ebrahimi  
 Institute for Drive Systems and Power Electronics, Leibniz  
 University Hannover, Welfengarten 1, 30167 Hannover,  
 Germany  
[martin.gerlach@ial.uni-hannover.de](mailto:martin.gerlach@ial.uni-hannover.de)

nungen verglichen, um die allgemeine Gültigkeit des ABM nachzuweisen.

**Schlüsselwörter** Elektrische Maschinen · Finite-Elemente-Methode · Magnetische Kerne · Numerische Berechnung · Analytische Berechnung · Stator · Schwingungen · Eigenfrequenzen · Eigenformen · Balkenelement

### Nomenclature

$A$	Cross-sectional area
$\mathbf{A}$	Assembly matrix
$\mathbf{D}$	Damping matrix
$D_i$	Inner yoke diameter
$D_o$	Outer yoke diameter
$E$	Young's modulus
$f$	Frequency
$\vec{F}$	Force vector
$h_y$	Yoke height
$h_t$	Tooth height
$h_{tt}$	Tooth tip height
$I$	Moment of inertia
$\mathbf{K}$	Stiffness matrix
$k$	Order of force wave
$l$	Element length
$l_s$	Stator length
$\mathbf{M}$	Mass matrix
$m$	Number of elements per tooth
$N_1$	Number of stator slots
$n$	Number of yoke elements per slot pitch
$q$	Number of degrees of freedom
$r$	Order of eigenmode
$t$	Time
$T$	Number of stator teeth
$u$	Displacement in direction $x$ or $t$
$v$	Displacement in direction $y$ or $r$
$w_t$	Tooth width
$w_{tt}$	Tooth tip width
$w_{so}$	Slot opening width
$\vec{x}$	Node displacement vector
$\alpha$	Angle between adjacent elements
$\gamma'$	Mechanical angle
$\rho$	Mass density
$\phi$	Bending angle
$\theta$	Angle between coordinate systems
$\vec{\Psi}$	Eigenvector
$\omega$	Angular frequency

## 1 Introduction

To determine the acoustic and vibration behavior of electric machines, the exciting magnetic forces in the air gap and the structural dynamic behavior of the machine must be calculated [1–4]. The forces in the air gap of the machine  $\vec{F}(\gamma', t)$  can be converted into force waves  $\vec{F}_k(\omega)$  with the order  $k$  describing the shape of the force wave. If the frequency and shape of a force wave coincide with an eigenmode and an eigenfrequency of the electric machine's sound rad-

iating parts, loud acoustic noise is emitted into the surroundings. Thus, the correct calculation in two domains, electromagnetic and structural dynamics, are important.

The vibration behavior of electric machines is characterized by the eigenfrequencies and eigenmodes of the sound radiating parts. The radiating parts are the stator, including the winding, and the housing. To calculate the vibration behavior, different approaches can be found in literature. Jordan and Frohne calculate the eigenfrequencies and eigenmodes using an analytical model based on a simplified circular ring of the machine's stator [1, 5]. The stator teeth and the winding are considered as additional mass. This model is expanded in the axial direction by Gieras [6]. In [7, 8], Verma and Girgis present a model that is based on the energy method. Another calculation approach is the finite-element (FE) method. The geometry is discretized into small elements for which the equations of motion are solved. The FE method allows the definition of different components, such as the winding and the housing, using different material models [9–13]. Due to its high accuracy, the FE method is widely used to calculate the vibration behavior of electric machines [3, 10–12, 14–17].

The analytical models and the FE method have certain advantages and disadvantages. The analytical models can be implemented easily, need low computational resources and provide fast results. However, the models only provide valid results if certain boundary conditions are fulfilled: the ratio  $\frac{h_y}{D_o}$  of the yoke height  $h_y$  to the outer diameter  $D_o$  must be small and the tooth eigenfrequencies must be significantly higher than the yoke eigenfrequencies. Furthermore, it is impracticable or at least difficult to include different components such as winding, teeth and housing in the model. The FE models can consider different geometries and components and can give more accurate results. However, they require high computational resources, a long modeling time and typically a software license.

To provide a fast and accurate calculation model that combines the advantages of the analytical models and the FE method, the so-called analytical beam element model (ABM) is introduced in [18]. The model is based on an *Euler-Bernoulli* beam element model that consists of two nodes, each with three degrees of freedom. The beams are used to build up a 2D model of the stator, including the stator yoke and teeth. The system's equation is derived from the beam element equations and is solved to determine the eigenfrequencies and eigenmodes. In [18], the ABM is validated using measurement results from the stator of a high-speed electric machine.

The goal of this work is to examine and extend the ABM further and to apply the model to machines of different sizes for validation. First, the basic approach of the ABM is summarized in Sect. 2. Then, different new approaches to the consideration of the sta-

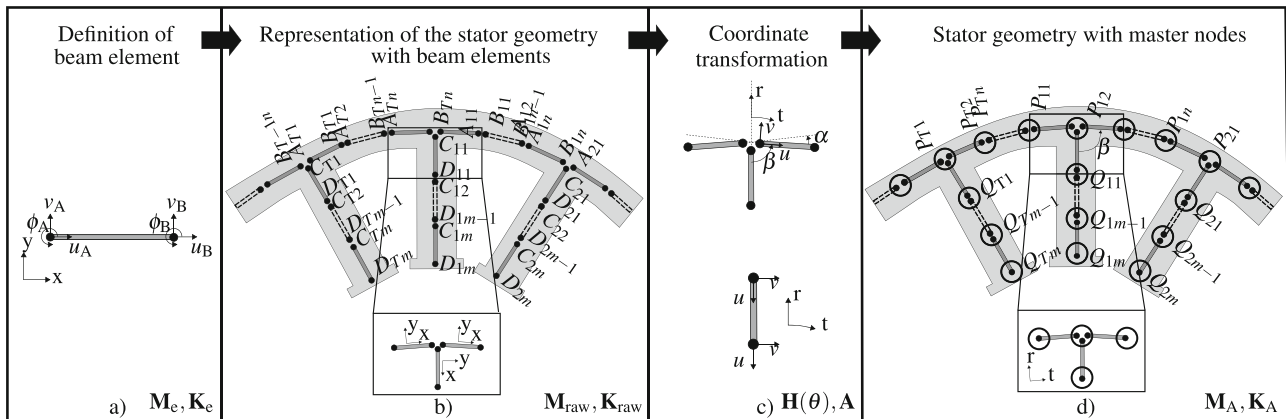


Fig. 1 Steps used to build up the analytical beam element model (ABM)

tor yoke's thickness are discussed in Sect. 3. These are the *Timoshenko* beam formulation, the multi-layer discretization of the yoke and a new feature which considers the lever arm effect of the stator teeth with respect to the yoke's intermediate surface, which are introduced in this paper. The results are compared to measurements and FE simulations in Sect. 4. In order to prove the general applicability of the ABM, the vibration behavior of four different stators with outer diameters ranging from 160 mm to 7 m are calculated. The results from these machines are compared to FE simulations in Sect. 5.

## 2 Analytical Beam Element Model – Basic Approach

In this section, the ABM is briefly introduced. A detailed description can be found in [18]. The individual steps employed to build the ABM are shown in Fig. 1 and described in the Sects. 2.2 to 2.5. First, the basic equation and the solution of a multi-mass oscillator are described in Sect. 2.1. Based on the basic approach of the ABM, the new modeling approaches are introduced.

### 2.1 Basic Equation of a Multi-Mass Oscillator

The stator of an electric machine can be described by a multi-mass oscillator. This is a multi-degree-of-freedom (DOF) system without gyroscopic effects that can be generally described by

$$\mathbf{M} \frac{d^2 \vec{x}(t)}{dt^2} + \mathbf{D} \frac{d \vec{x}(t)}{dt} + \mathbf{K} \vec{x}(t) = \vec{F}, \quad (1)$$

where  $\mathbf{M}$ ,  $\mathbf{D}$  and  $\mathbf{K}$  are the mass, damping and stiffness matrices, respectively.  $\vec{F}$  is the vector of the applied forces and  $\vec{x}$  is the vector of displacements for each DOF.

The system can be decomposed and diagonalized in terms of its eigenvectors  $\vec{\Psi}_r$ , also known as its eigenmodes, and the corresponding eigenfrequencies

$f_{0,r}$ . The eigenfrequencies  $\omega_{0,r} = 2\pi f_{0,r}$  are calculated by solving

$$\det(-\omega_0^2 \mathbf{M} + \mathbf{K}) = 0, \quad (2)$$

which will provide  $q$  solutions for a system with  $q$  DOFs.  $r$  is the order of the eigenmodes. In case of a cylindrical structure such as the stator of an electric machine, the order  $r$  represents the number of maxima or minima around the circumference.

The eigenvectors  $\vec{\Psi}_r$  are determined by replacing each of the  $q$  obtained eigenfrequencies in (1), rewritten in the frequency domain with no damping and no external forces. The base transformation or modal matrix  $\Psi$  is then defined as the matrix formed by the  $q$  eigenvectors placed in its columns

$$\Psi = [\vec{\Psi}_1, \vec{\Psi}_2, \dots, \vec{\Psi}_q]. \quad (3)$$

The relationship between the vectors  $\vec{x}$  (in the original base) and  $\vec{X}$  (in the transformed base) is given by

$$\vec{x} = \Psi \vec{X}. \quad (4)$$

Since the eigenvectors provide only the directions of the new vector base, they can be arbitrarily scaled. Typically, the mass matrix is used for the scaling, giving the relations

$$\Psi^T \mathbf{M} \Psi = \mathbf{I} = \text{diag}(1) \quad (5)$$

$$\Psi^T \mathbf{K} \Psi = \omega_0^2 = \text{diag}(\omega_{0,r}^2) \quad (6)$$

$$\Psi^T \mathbf{D} \Psi = \mathbf{D}' = \text{diag}(2d_r \omega_{0,r}) \quad (7)$$

where  $r = 1 \dots q$ . In (7), it is assumed that the damping matrix can be approximated as a linear combination of the mass and stiffness matrices, and  $d_r$  is the modal damping factor for eigenmode  $r$ . As a result,

the decoupled system equations in the transformed base become

$$(-\omega^2 \mathbf{I} + j\omega \mathbf{D}' + \omega_0^2) \tilde{\mathbf{X}}(\omega) = \Psi^T \tilde{\mathbf{F}}(\omega). \quad (8)$$

Using this equation, the vibration response  $\tilde{\mathbf{x}}$  to a force excitation  $\tilde{\mathbf{F}}$  of the system can be calculated. This procedure forms the basis of the vibration and acoustic analysis. The purpose of the ABM is to describe the mass and stiffness matrices and to calculate the eigenfrequencies and eigenmodes.

### 2.2 Euler-Bernoulli Beam Element

In the basic approach introduced in [18], the *Euler-Bernoulli* beam element, as represented in Fig. 1a, is used to discretize the stator of an electric machine and to generate the mass and stiffness matrices.

The stiffness matrix  $\mathbf{K}_e$  for such a beam element with three DOFs per node is

$$\mathbf{K}_e = \begin{bmatrix} \frac{EA}{l} & 0 & 0 & -\frac{EA}{l} & 0 & 0 \\ 0 & \frac{12EI}{l^3} & \frac{6EI}{l^2} & 0 & -\frac{12EI}{l^3} & \frac{6EI}{l^2} \\ 0 & \frac{6EI}{l^2} & \frac{4EI}{l} & 0 & -\frac{6EI}{l^2} & \frac{2EI}{l} \\ -\frac{EA}{l} & 0 & 0 & \frac{EA}{l} & 0 & 0 \\ 0 & -\frac{12EI}{l^3} & -\frac{6EI}{l^2} & 0 & \frac{12EI}{l^3} & -\frac{6EI}{l^2} \\ 0 & \frac{6EI}{l^2} & \frac{2EI}{l} & 0 & -\frac{6EI}{l^2} & \frac{4EI}{l} \end{bmatrix}. \quad (9)$$

$E$  is the material's *Young's* modulus,  $l$  is the beam element length,  $A$  is the cross-sectional area and  $I$  is the moment of inertia of the beam [19]. Shear strains are neglected in this formulation. Similarly, the element's mass matrix  $\mathbf{M}_e$  is defined as

$$\mathbf{M}_e = \frac{\rho Al}{420} \begin{bmatrix} 140 & 0 & 0 & 70 & 0 & 0 \\ 0 & 156 & 22l & 0 & 54 & -13l \\ 0 & 22l & 4l^2 & 0 & 13l & -3l^2 \\ 70 & 0 & 0 & 140 & 0 & 0 \\ 0 & 54 & 13l & 0 & 156 & -22l \\ 0 & -13l & -3l^2 & 0 & -22l & 4l^2 \end{bmatrix}, \quad (10)$$

where  $\rho$  is the beam material's mass density [19]. The mass and stiffness matrices are defined by considering the node DOFs shown in Fig. 1a as a vector written in the sequence  $[u_A, v_A, \phi_A, u_B, v_B, \phi_B]^T$ .

### 2.3 Representation of the Stator Geometry with Beam Elements

The cross-sectional area of the elements in the yoke corresponds to the stator's axial length  $l_s$  multiplied by the yoke height  $h_y$ . The cross-section of the elements which represent the teeth is assumed to be constant and is defined by the stator's axial length and the average width of the teeth. In case the teeth have tips with a larger width, the tip's additional mass is accounted

for by increasing the mass density of the last element of each tooth.

Initially, the elements are not connected to each other. This way, the free element equations, using their own local coordinate systems, can be written by replicating the single-element mass and stiffness matrices on the diagonal of a global matrix. This procedure produces the stiffness matrix  $\mathbf{K}_{\text{raw}}$  and the mass matrix  $\mathbf{M}_{\text{raw}}$  [18].

### 2.4 Coordinate Transformation

The next step is to connect the beam elements to each other. This is achieved by means of defined master nodes named  $P_{11} \dots P_{Tn}$  and  $Q_{11} \dots Q_{Tm}$ , which use a cylindrical coordinate system and correlate with the beam nodes  $A, B, C$ , and  $D$ , as illustrated in Fig. 1c. The relation between an arbitrary element node  $EN$  in its local coordinate system and a corresponding master node  $MN$  in cylindrical coordinates is

$$\begin{bmatrix} u_{EN} \\ v_{EN} \\ \phi_{EN} \end{bmatrix} = \underbrace{\begin{bmatrix} -\sin\theta & \cos\theta & 0 \\ \cos\theta & \sin\theta & 0 \\ 0 & 0 & 1 \end{bmatrix}}_{\mathbf{H}(\theta)} \underbrace{\begin{bmatrix} u_{MN} \\ v_{MN} \\ \phi_{MN} \end{bmatrix}}_{\tilde{\mathbf{x}}_{MN}}. \quad (11)$$

$\theta$  is the angle between the  $r$  and  $y$  axes of the cylindrical and local coordinate systems. Based on the trigonometric relations shown in Fig. 1c, the transformation matrices are calculated as

$$\mathbf{H}_A = \mathbf{H}\left(\frac{\alpha}{2}\right); \quad \mathbf{H}_B = \mathbf{H}\left(-\frac{\alpha}{2}\right); \quad \mathbf{H}_C = \mathbf{H}_D = \mathbf{H}\left(\frac{\pi}{2}\right) \quad (12)$$

for nodes  $A, B, C$ , and  $D$ , respectively. The angle  $\alpha$  is the angle between adjacent elements in the stator yoke.

### 2.5 Stator Geometry with Master Nodes

Based on this, a complete nodal transformation from ABCD (element nodes) to PQ (master nodes) is performed by

$$\underbrace{\begin{bmatrix} \tilde{\mathbf{x}}_{A11} \\ \tilde{\mathbf{x}}_{B11} \\ \tilde{\mathbf{x}}_{A12} \\ \tilde{\mathbf{x}}_{B12} \\ \vdots \\ \tilde{\mathbf{x}}_{C11} \\ \tilde{\mathbf{x}}_{D11} \\ \tilde{\mathbf{x}}_{C12} \\ \tilde{\mathbf{x}}_{D12} \\ \vdots \end{bmatrix}}_{\tilde{\mathbf{x}}_{ABCD}} = \underbrace{\begin{bmatrix} \mathbf{H}_A & 0 & \dots & & 0 & \dots \\ 0 & \mathbf{H}_B & & & & \\ \vdots & \mathbf{H}_A & & & & \\ & & \mathbf{H}_B & & & \\ & & & \dots & & \\ \mathbf{H}_C & & & & & \\ & & & & \mathbf{H}_D & \\ & & & & \mathbf{H}_C & \\ 0 & & & & & \mathbf{H}_D \\ \vdots & & & & & \ddots \end{bmatrix}}_A \underbrace{\begin{bmatrix} \tilde{\mathbf{x}}_{P11} \\ \tilde{\mathbf{x}}_{P12} \\ \tilde{\mathbf{x}}_{P13} \\ \vdots \\ \tilde{\mathbf{x}}_{Q11} \\ \tilde{\mathbf{x}}_{Q12} \\ \vdots \\ \tilde{\mathbf{x}}_{PQ} \end{bmatrix}}_{\tilde{\mathbf{x}}_{PQ}} \quad (13)$$

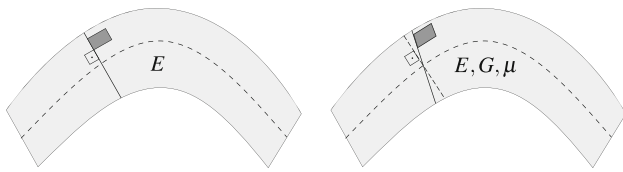


Fig. 2 Beam element behavior in deformation. **a** Euler-Bernoulli beam, **b** Timoshenko beam

$\mathbf{A}$  is the assembly matrix obtained by combining the previously defined transformation matrices  $\mathbf{H}_A$ ,  $\mathbf{H}_B$ ,  $\mathbf{H}_C$  and  $\mathbf{H}_D$ , surrounded by zeros. The final system stiffness matrix  $\mathbf{K}_A$  and mass matrix  $\mathbf{M}_A$  of the connected beams become

$$\mathbf{K}_A = \mathbf{A}^T \cdot \mathbf{K}_{\text{raw}} \cdot \mathbf{A}, \quad (14)$$

and

$$\mathbf{M}_A = \mathbf{A}^T \cdot \mathbf{M}_{\text{raw}} \cdot \mathbf{A}. \quad (15)$$

These two matrices are used for calculating the stator eigenmodes and eigenfrequencies according to the procedure described in Sect. 2.1.

### 3 Different Modeling Approaches

Different approaches are investigated for taking into account the effect of the stator yoke's thickness on the eigenmodes and eigenfrequencies. These approaches use the *Timoshenko* beam element or the multi-layer structure which are presented and compared in the following subsections. Furthermore, a translation transformation is introduced to consider the lever arm effect of the stator teeth on the yoke's intermediate surface.

#### 3.1 Timoshenko Beam

The first approach involves to replace the *Euler-Bernoulli* beam element used in [18] with the *Timoshenko* beam element. The *Euler-Bernoulli* beam element assumes that the beam cross-section remains perpendicular to the beam's intermediate axis when deformed. This assumption neglects the shear deformations and is typically suitable for problems where the beam thickness is relatively small compared to its length. The *Timoshenko* formulation allows the beam cross-section to rotate with respect to the intermediate axis and, therefore, takes into account possible shear deformations. This allows the method to account for the natural tendency of the cross-section to rotate back to its initial position, relieving the internal stresses and making the *Timoshenko* formulation suitable for moderately thick beams. Fig. 2 illustrates the assumptions made using the two formulations discussed.

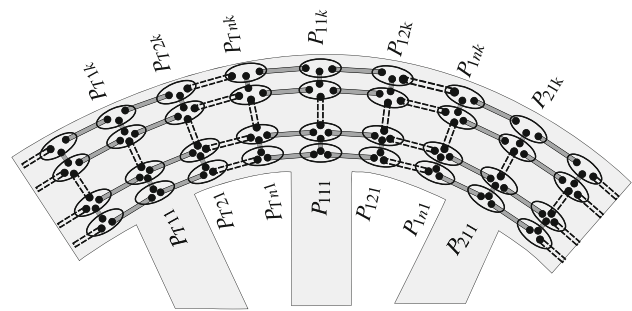


Fig. 3 Representation of the multi-layer structure of the beam elements in the stator yoke

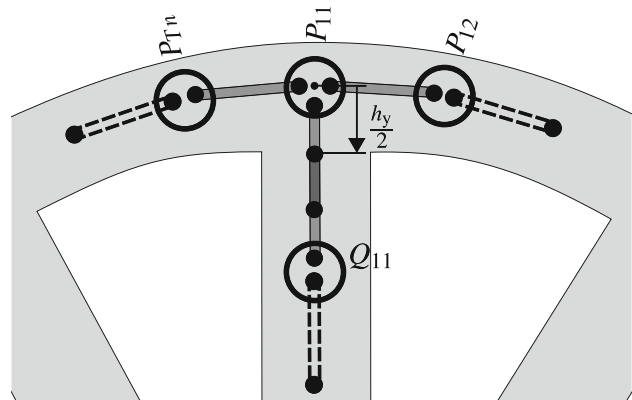


Fig. 4 Modeling of the connection of the stator teeth and the stator yoke

According to the *Timoshenko* formulation, the mass matrix

$$\mathbf{M}_e = \mathbf{M}_{\text{trans}} + \mathbf{M}_{\text{rot}} \quad (16)$$

can be written as the sum of the translational mass  $\mathbf{M}_{\text{trans}}$  and the rotational mass  $\mathbf{M}_{\text{rot}}$ . Together with the corresponding stiffness mass  $\mathbf{K}_e$  they are [19]

$$\mathbf{M}_{\text{trans}} = \frac{\rho A l}{210(1+\gamma)^2} \begin{bmatrix} 70(1+\gamma)^2 & 0 & 0 & 35(1+\gamma)^2 & 0 & 0 \\ 0 & (70\gamma^2 + 147\gamma + 78) & (35\gamma^2 + 77\gamma + 44)\frac{l}{4} & 0 & (35\gamma^2 + 63\gamma + 27) & -(35\gamma^2 + 63\gamma + 26)\frac{l}{4} \\ 0 & (35\gamma^2 + 77\gamma + 44)\frac{l}{4} & (7\gamma^2 + 14\gamma + 8)\frac{l^2}{4} & 0 & (35\gamma^2 + 63\gamma + 26)\frac{l}{4} & -(7\gamma^2 + 14\gamma + 6)\frac{l^2}{4} \\ 35(1+\gamma)^2 & 0 & 0 & 70(1+\gamma)^2 & 0 & 0 \\ 0 & (35\gamma^2 + 63\gamma + 27) & (35\gamma^2 + 63\gamma + 26)\frac{l}{4} & 0 & (70\gamma^2 + 147\gamma + 78) & -(35\gamma^2 + 77\gamma + 44)\frac{l}{4} \\ 0 & -(35\gamma^2 + 63\gamma + 26)\frac{l}{4} & -(7\gamma^2 + 14\gamma + 6)\frac{l^2}{4} & 0 & -(35\gamma^2 + 77\gamma + 44)\frac{l}{4} & (7\gamma^2 + 14\gamma + 8)\frac{l^2}{4} \end{bmatrix}, \quad (17)$$

$$\mathbf{M}_{\text{rot}} = \frac{\rho I}{30(1+\gamma)^2 l} \begin{bmatrix} 0 & 0 & 0 & 0 & 0 & 0 \\ 0 & 36 & -(15\gamma - 3)l & 0 & -36 & -(15\gamma - 3)l \\ 0 & -(15\gamma - 3)l & (10\gamma^2 + 5\gamma + 4)l^2 & 0 & (15\gamma - 3)l & (5\gamma^2 - 5\gamma - 1)l^2 \\ 0 & 0 & 0 & 0 & 0 & 0 \\ 0 & -36 & (15\gamma - 3)l & 0 & 36 & (15\gamma - 3)l \\ 0 & -(15\gamma - 3)l & (5\gamma^2 - 5\gamma - 1)l^2 & 0 & (15\gamma - 3)l & (10\gamma^2 + 5\gamma + 4)l^2 \end{bmatrix}, \quad (18)$$

and

$$\mathbf{K}_e = C \cdot \begin{bmatrix} \frac{Al^2}{I}(1+\gamma) & 0 & 0 & -\frac{Al^2}{I}(1+\gamma) & 0 & 0 \\ 0 & 12 & 6l & 0 & -12 & 6l \\ 0 & 6l & (4+\gamma)l^2 & 0 & -6l & (2-\gamma)l^2 \\ -\frac{Al^2}{I}(1+\gamma) & 0 & 0 & \frac{Al^2}{I}(1+\gamma) & 0 & 0 \\ 0 & -12 & -6l & 0 & 12 & -6l \\ 0 & 6l & (2-\gamma)l^2 & 0 & -6l & (4+\gamma)l^2 \end{bmatrix}. \quad (19)$$

$C$  and  $\gamma$  are defined by

$$C = \frac{EI}{(1+\gamma)l^3} \text{ and } \gamma = \frac{12}{l^2} \left( \frac{EI}{\kappa GA} \right). \quad (20)$$

$\kappa$  is the shear correction factor used to consider the non-uniform shear distributions. It is typically assumed to be 5/6 [19].  $G$  is the shear modulus. Under the assumption that the material is isotropic, this can be calculated as [20]

$$G = \frac{E}{2(1+\mu)}. \quad (21)$$

$\mu$  is the Poisson's ratio. When considering an isotropic material, the material is defined if two of the three quantities  $E$ ,  $G$  and  $\mu$  are known. It is worth noting that (9) and (10) from the investigation of the *Euler-Bernoulli* beam correspond to a particular case of the *Timoshenko* beam in which the shear modulus  $G$  tends to infinity.

### 3.2 Multi-Layer Structure

Another possible approach to considering the stator yoke's thickness accurately is to discretize the yoke with multiple *Euler-Bernoulli* beam element layers, as represented in Fig. 3. The layers are connected to each

other by vertical beam elements with a cross-section dependent on the number of elements around the circumference and a length dependent on the number of layers. It is worth noting that the vertical elements' masses would overlap with that of the yoke elements, since they occupy the same volume. Therefore, the mass density of all the vertical elements in the yoke is set to zero, so that they act solely as an ideal elastic connection between the layers.

This approach also requires an extension of the assembly matrix  $\mathbf{A}$  defined in (13) to consider the connection of the newly introduced beams. The extensions are made following the same principle as presented in Sect. 2.2.

### 3.3 Tooth Connection Modeling

Since the beam elements representing the stator yoke correspond to the yoke's intermediate surface, a direct connection between the tooth base and the yoke nodes would produce a partial overlap of the tooth and yoke beam elements. Taking the yoke height as  $h_y$ , the overlapping height is  $\frac{h_y}{2}$  as illustrated in Fig. 4. Evidently, this fact becomes more relevant for the case of a thick stator yoke.

In this work, an additional translational transformation of the master nodes  $P$  is considered as means to connect the nodes of the tooth bases to the yoke. This translation corresponds to the lever arm effect of the yoke cross-section modeled as a rigid body when it rotates. For an arbitrary translation of  $(\Delta x, \Delta y)$  applied to a point  $P'$  with respect to the point  $P$ , the transformation matrix  $\mathbf{T}(\Delta x, \Delta y)$  can be defined as

$$\underbrace{\begin{bmatrix} u_{P'} \\ v_{P'} \\ \phi_{P'} \end{bmatrix}}_{\tilde{x}_{P'}} = \underbrace{\begin{bmatrix} 1 & 0 & -\Delta y \\ 0 & 1 & \Delta x \\ 0 & 0 & 1 \end{bmatrix}}_{\mathbf{T}(\Delta x, \Delta y)} \underbrace{\begin{bmatrix} u_P \\ v_P \\ \phi_P \end{bmatrix}}_{\tilde{x}_P}. \quad (22)$$

In combination with the rotation matrix presented in (11), a generalized coordinate transformation including translations and rotation effects can be defined as the multiplication  $\mathbf{H}(\theta) \cdot \mathbf{T}(\Delta x, \Delta y)$ . For the connection of the nodes in the tooth base to the yoke, for instance, the transformation matrix is calculated using  $\theta = \frac{\pi}{2}$ ,  $\Delta x = 0$  and  $\Delta y = \frac{-h_y}{2}$ . Such complete transformation can be considered when generating the assembly matrix  $\mathbf{A}$ , as explained in (13), so that the lever arm effect of the tooth base with respect to the yoke's intermediate surface can be taken into account.

#### 4 Comparison of the Modeling Approaches

For a comparison of the modeling approaches described in Sect. 3, the stator S1 shown in Table 1 will be used. At first, only the stator yoke without the teeth is analyzed. This allows the evaluation of the different methods for considering the yoke height without the effect of the teeth. Then, the complete model with the teeth is calculated using the ABM and is compared with measurements and FE simulations. The results of the FE simulations and the measurements have already been presented in [10, 21].

##### 4.1 Stator Yoke

Table 2 summarizes the results of the ABM with the *Euler-Bernoulli* (EB) beam, the *Timoshenko* (TS) beam and the multi-layer (ML) approach to modeling the stator yoke. 120 elements are considered around the circumference for all the ABM models and the multi-layer model is calculated with two layers. The results are compared to the FE simulation results and the deviations  $f_{\Delta,r,EB/TS/ML} = \frac{f_{0,r,EB/TS/ML} - f_{0,r,FE}}{f_{0,r,FE}}$  between the individual approaches (EB/TS/ML) and the FE model are determined.


It can be seen that the model with the *Euler-Bernoulli* beam element produces the highest deviations  $f_{\Delta,r}$  when compared to the FE model. This is due to the fact that the shear strains are neglected in this method, which is appropriate for slender beams but becomes less accurate when the thickness of the beam increases in relation to its length. The ratio of

the yoke height  $h_y$  to the mean stator diameter  $D_o$  is 0.103 for the stator S1. In this case, the results calculated using the *Timoshenko* beam element and the multi-layer approach are more accurate. Although these two aforementioned methods present similar deviations for the case studied ( $f_{\Delta,r} = 0.02\% \dots 4.88\%$ ), the *Timoshenko* approach is the one which offers more advantages. One is that it requires less elements than the multi-layer approach, since only one layer is necessary. Another is that the effect of the shear strain is intrinsically considered in the constituent equations of the *Timoshenko* beam, whereas, in the multi-layer approach, this is accounted for by means of the virtual vertical beams connecting the layers. As a consequence, the stiffness for shear displacements between the layers becomes dependent on the number of elements in the system in such a way that an excessive number of elements (with consequently very thin vertical beams) would produce a model which underestimates the shear stiffness. Accordingly, the multi-layer approach leads to different results for different numbers of vertical beam elements.

##### 4.2 Stator Yoke with Teeth

In Table 3, the results for the stator with teeth are summarized and compared to measurements and results of the FE simulations. In this case, only the ABM with the *Timoshenko* beam element is considered since, as

**Table 1** Data concerning the stator S1

Geometric data		Material data	
Stator length $l_s$	110 mm	Mass density	7400 $\frac{\text{kg}}{\text{m}^3}$
Outer diameter $D_o$	160 mm	Young's modulus	190 GPa
Inner diameter $D_i$	82 mm	Poisson's ratio	0.3
Number of slots $N_1$	24		Picture of stator S1
Tooth width $w_t$	4.7 mm		
Tooth height $h_t$	22.5 mm		
Tooth tip width $w_{tt}$	8.92 mm		
Tooth tip height $h_{tt}$	2 mm		

**Table 2** Calculated eigenfrequencies of the stator yoke using the *Euler* beam element, *Timoshenko* beam element and multi-layer approach compared to FE calculations

Eigenpairs	$r = 2$	$r = 3$	$r = 4$	$r = 0$	$r = 5$
$f_{0,r,FE}$ in Hz	1952	5319	9721	11 293	14 890
$f_{0,r,EB}$ in Hz	1991	5623	10 771	11 241	17 407
$f_{\Delta,r,EB}$ in %	+2.0	+0.13	+10.8	-0.45	+16.9
$f_{0,r,TS}$ in Hz	1953	5367	9924	11 241	15 396
$f_{\Delta,r,TS}$ in %	+0.05	+0.90	+2.09	-0.46	+3.40
$f_{0,r,ML}$ in Hz	1909	5128	9280	11 295	14 162
$f_{\Delta,r,ML}$ in %	-2.20	-3.59	-4.54	+0.02	-4.88

discussed in Sect. 4.1, this produces better results for the modeling of the stator yoke's thickness. The ABMs are composed of 120 elements in the yoke and 5 elements per tooth. Two variants of the *Timoshenko* approach are compared: one including the effect of the lever arm discussed in Sect. 3.3 (TS,LA) and another one neglecting this effect (TS).

Furthermore, the results are compared to the FE model and to results of an experimental modal analysis. The experimental modal analysis is performed by means of an instrumented hammer and one accelerometer installed in the back of the yoke. Details concerning the test procedure and the results obtained can be found in the related papers [10, 21].

The deviations  $f_{\Delta,r}$  shown in Table 3 are calculated with respect to the measured values. An exception is made for the eigenmode  $r = 5$ , which could not be identified in the measurements due to its high frequency (see [10, 21]). In this case, the deviations marked with an asterisk (\*) are calculated with respect to the FE model.

In general, it can be seen that the calculated eigenfrequencies show a good agreement with the measurements, with a maximum absolute deviation of 7.43%. Nevertheless, the deviations are generally lower when the lever arm effect discussed in Sect. 4.1 is taken into account. This becomes more evident for the mode  $r = 4$ , where large deflections of the teeth are present, as can be seen in Table 5. The absolute deviation decreases from 7.43% to 4.06% when the lever arm effect is considered.

## 5 Vibration Behavior of Different Stator Geometries

In this section, the ABM is used to calculate the vibration behavior of four different stators. The stators are shown in Table 4 together with their geometric and material data. The outer diameter of the stators ranges from  $D_o = 160$  mm to  $D_o = 7$  m and the number of teeth ranges from  $N_1 = 24$  to  $N_1 = 480$ .

The stator S1 has already been introduced in Sect. 4 and is used in a high-speed electric machine for a traction application [22]. Stators S2, S3 and S4 are taken from real applications. The stator S2 is derived from a conventional electric machine for a traction appli-

cation. The stator S3 is derived from a prototype hydrogenerator and the stator S4 from a real operational hydrogenerator.

The vibration behavior of the four stators is calculated using 2D FE models. The material data in Table 4 is used for the simulations. The results of the FE calculations are used as a reference for the results calculated with the improved ABM using the *Timoshenko* beam element, including the lever arm effect of the teeth relative to the yoke. The eigenmodes  $\bar{\Psi}_r$ , the eigenfrequencies  $f_{0,r}$  and their deviations  $f_{\Delta,r}$  are given in Table 5.

### 5.1 Stator S1

The eigenfrequencies of the eigenmodes  $r = 2$ ,  $r = 3$ ,  $r = 0$ ,  $r = 4$  and  $r = 5$  of stator S1 are shown in Table 5. As discussed in Sect. 4, the deviations are lower than 5%. The eigenmodes calculated using the ABM show a good accordance with the eigenmodes calculated using the FE model. Beside the eigenmode  $r = 0$ , the deviations  $f_{\Delta,r}$  between the ABM and the FE model are negative, indicating that the ABM is tendentially less stiff than the FE model in this case.

### 5.2 Stator S2

Due to the larger size of stator S2, its eigenfrequencies are reduced in comparison to stator S1. According to the conclusions of Jordan [1], the bending eigenmodes  $r = 2$ ,  $r = 3$ ,  $r = 4$ ,  $r = 5$  of the stator are reduced more sharply than the eigenmode  $r = 0$  due to the increased size of the machine. The deviations  $f_{\Delta,r}$  between the calculated eigenfrequencies of the ABM and the FE models are lower than 2%, except for eigenmode  $r = 5$ . For the eigenmode  $r = 5$ , the deviation is around 6%. The calculated eigenmodes show a good accordance. For the stator S2, the deviations between the ABM and the FE model are both negative or positive.

### 5.3 Stator S3

The eigenmodes and eigenfrequencies of stator S3 show a good accordance between the ABM and the FE model. The deviations between the eigenfrequencies  $f_{\Delta,r}$  are lower than 3% (see Table 5). It is striking that the deviations are all negative. In comparison to stators S1 and S2, the eigenfrequencies are lower due to the larger size of the stator.

### 5.4 Stator S4

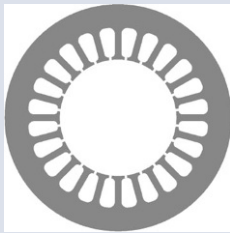
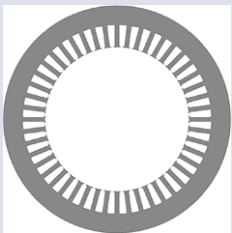
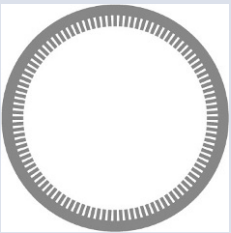
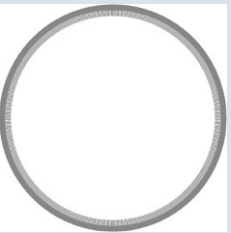
The calculated eigenmodes and eigenfrequencies of stator S4 confirm the results so far. The deviations between the ABM and FE model  $f_{\Delta,r}$  are lower than 1.5%. Accordingly, it can be concluded that the ABM and the FE model show a very high accordance. As with the stator S3, the deviations  $f_{\Delta,r}$  are all negative (see Table 5).

**Table 3** Calculated eigenfrequencies of the stator using the *Timoshenko* beam element and lever arm approach compared to FE calculations and measurement results

Eigenpairs	$r = 2$	$r = 3$	$r = 0$	$r = 4$	$r = 5$
$f_{0,r,meas}$ in Hz	1639	4048	9571	10 101	n.a.
$f_{0,r,FE}$ in Hz	1638	4061	9511	10 081	13 952
$f_{\Delta,r,FE}$ in %	-0.06	+0.32	-0.63	-0.2	n.a.
$f_{0,r,TS}$ in Hz	1612	4185	9568	9351	13 589
$f_{\Delta,r,TS}$ in %	-1.65	3.38	-0.03	-7.43	-2.60*
$f_{0,r,TS,LA}$ in Hz	1568	3935	9568	9691	13 621
$f_{\Delta,r,TS,LA}$ in %	-4.33	-2.79	-0.03	-4.06	-2.37*



Table 4 Geometric and material data concerning the four stators

Stator	S1	S2	S3	S4
				
<b>Geometric data</b>				
Stator length $l$	110 mm	220 mm	330 mm	1300 mm
Outer diameter $D_o$	160 mm	230 mm	1600 mm	7000 mm
Inner diameter $D_i$	82 mm	145 mm	1292 mm	6280 mm
Number of slots $N_1$	24	48	108	480
Tooth width $h_{tw}$	4.7 mm	5 mm	25 mm	26 mm
Tooth height $h_{tw}$	22.5 mm	24 mm	77 mm	180 mm
Slot opening width $h_{th}$	2 mm	2 mm	12 mm	15 mm
Tooth tip width $h_{ttw}$	8.92 mm	7.49 mm	–	–
Tooth tip height $h_{tth}$	2 mm	1 mm	–	–
Ratio $\frac{h_y}{D_o}$	0.103	0.08	0.048	0.026
<b>Material data</b>				
Mass density $\rho$			7400 $\frac{\text{kg}}{\text{m}^3}$	
Young's modulus $E$			190 GPa	
Poisson's ratio $\mu$			0.3	

The comparison of the four stators' vibration behavior using the ABM and the FE model proves that the ABM is capable of correctly predicting the vibration behavior of electric machines with outer diameters from  $D_o = 160$  mm to  $D_o = 7$  m. Despite the eigenfrequency  $f_{r=5}$  of stator S2, the deviation  $f_{\Delta,r}$  is lower than 5%, indicating a good agreement between the ABM and the respective FE model.

The deviations between the ABM and the FE model are mainly negative. This indicates that the ABM tends to be less stiff than the FE method. Furthermore, it is noteworthy that the deviation  $f_{\Delta,r}$  decreases with increasing size of the machine. To analyze this, the mean deviation  $\bar{f}_{\Delta} = \frac{\sum_{r=1}^{r_{\max}} |f_{\Delta,r}|}{n_r}$  is calculated.

The ratio  $\frac{h_y}{D_o}$  between the yoke height and the outer diameter decreases with increasing size as well (see Table 4). Accordingly, the influence of the shear strain in the stator yoke is higher for machines with a high ratio of  $\frac{h_y}{D_o}$ . The shear strain is only approximated by the *Timoshenko* beam element and is better described by the FE models. Thus, the deviations between the FEM and ABM decrease with increasing size of the stators S1 to S4. These observations can also be made when calculating the vibration behavior using the analytical model of Jordan [1]. This analytical model is not capable of correctly calculating the vibration behavior of small machines with a high ratio of  $\frac{h_y}{D_o}$ . For machines with a small ratio of  $\frac{h_y}{D_o}$ , the analytical model leads to better results. Accordingly, the correct

description of the stator yoke's vibration behavior is the major challenge in the calculation of the vibration behavior for machines with a high ratio of  $\frac{h_y}{D_o}$ . It can be concluded that the approach presented, using the *Timoshenko* beam element model, is capable of calculating the vibration behavior of machines of different sizes, taking into account the vibration behavior of the stator yoke.

## 6 Conclusion

In this paper, the ABM originally presented in [18] is examined and expanded further. Different modeling approaches are investigated to enhance the calculation accuracy of the ABM and the model is applied to machines of different sizes for validation.

One major challenge is the correct description of the stator yoke's thickness and its influence on the vibration behavior. To consider this effect in the ABM, two different approaches are compared in this work: the use of the *Timoshenko* beam element and the modeling of the stator using a multi-layer structure. Furthermore, the model is enhanced by adding a feature which considers the lever arm effect of the stator teeth with respect to the yoke's intermediate surface.

When comparing the results of the ABM with FE and measurement results, it can be concluded that the use of the *Timoshenko* beam element is the best means to consider the stator yoke's thickness. The modeling approach using a multi-layer structure does

Table 5 Eigenfrequencies of the ABM compared to the FE models

Eigenpairs	S1						S2					
	$r=2$	$r=3$	$r=0$	$r=4$	$r=5$	$\bar{f}_\Delta$	$r=2$	$r=3$	$r=4$	$r=5$	$r=0$	$\bar{f}_\Delta$
$\Psi_{r,FE}$												
$f_{0,r,FE}$ in Hz	1638	4061	9511	10 081	13 952		812	2143	3666	4808	6238	
$\Psi_{r,ABM}$												
$f_{0,r,ABM}$ in Hz	1568	3935	9568	9691	13 621		798	2123	3718	5100	6259	
$f_{\Delta,r}$ in %	-4.27	-3.10	+0.60	-3.87	-2.37	2.84	-1.72	-0.93	+1.42	+6.07	-1.11	2.25
	S3						S4					
	$r=2$	$r=3$	$r=4$	$r=5$	$r=0$	$\bar{f}_\Delta$	$r=2$	$r=3$	$r=4$	$r=5$	$r=0$	$\bar{f}_\Delta$
$\Psi_{r,FE}$												
$f_{0,r,FE}$ in Hz	66.1	182.7	341.9	536.8	848.4		7.7	21.5	40.9	65.6	188.1	
$\Psi_{r,ABM}$												
$f_{0,r,ABM}$ in Hz	64.4	178.4	334.8	527.8	846.4		7.6	21.3	40.5	65.0	188.0	
$f_{\Delta,r}$ in %	-2.57	-2.35	-2.08	-1.68	-0.24	1.75	-1.3	-0.93	-0.98	-0.91	-0.11	0.85

not lead to convincing results, since the model accuracy depends on the number of vertical beam elements used. Additionally, the feature which considers the lever arm effect of the stator teeth increases the calculation accuracy yet further.

In order to validate the method presented for a large range of applications, the improved ABM, using the *Timoshenko* beam element and considering the lever arm effect, is used to calculate the vibration behavior of four stator cores of different sizes. The results are compared to FE results and show a high accordance. The deviation of the eigenfrequencies is mostly less than 5%. It is noteworthy that the deviation between the ABM and FE even decreases with increasing size of the machines. For the stator S4, the deviation of the eigenfrequencies is even lower than 1.5%.

Overall, the measures presented in this work improve the calculation quality of the ABM further and enable it to calculate the vibration behavior of machines of different sizes.

The ABM can be used in combination with calculated electromagnetic forces to predict the machine's vibration during operation. Furthermore, the model has the potential to be extended to include the winding and the stator's frame or housing, and also to be expanded in the axial direction, allowing it to consider axial eigenmodes.

**Funding** Open Access funding enabled and organized by Projekt DEAL.

**Open Access** This article is licensed under a Creative Commons Attribution 4.0 International License, which permits use, sharing, adaptation, distribution and reproduction in any medium or format, as long as you give appropriate credit

to the original author(s) and the source, provide a link to the Creative Commons licence, and indicate if changes were made. The images or other third party material in this article are included in the article's Creative Commons licence, unless indicated otherwise in a credit line to the material. If material is not included in the article's Creative Commons licence and your intended use is not permitted by statutory regulation or exceeds the permitted use, you will need to obtain permission directly from the copyright holder. To view a copy of this licence, visit <http://creativecommons.org/licenses/by/4.0/>.

## References

- Jordan H (1950) Der geräuscharme Elektromotor. Girardet, Essen
- Braunisch D, Ponick B, Bramerdorfer G (2013) Combined analytical–numerical noise calculation of electrical machines considering nonsinusoidal mode shapes. *IEEE Trans Magn* 49(4):1407–1415
- Vip S-A, Hollmann J, Ponick B (2019) Nvh-simulation of salient-pole synchronous machines for traction applications. In: Proceedings 2019 International Aegean Conference on Electrical Machines and Power Electronics (ACEMP) & 2019 International Conference on Optimization of Electrical and Electronic Equipment (OPTIM). IEEE, Piscataway, pp 246–253
- Hofmann A, Qi F, Lange T, de Doncker RW (2014) The breathing mode-shape 0: Is it the main acoustic issue in the pmsms of today's electric vehicles? In: 17th International Conference on Electrical Machines and Systems (ICEMS). IEEE, Piscataway, pp 3067–3073
- Frohne H (1959) *Über die primäre Bestimmungsgrößen der Lautstärke bei Asynchronmaschinen*. Dissertation thesis, Technische Hochschule Hannover, Hannover
- Gieras JE, Wang C, Lai JC (2006) Noise of polyphase electric motors, volume 129 of Electrical and computer engineering. CRC/Taylor & Francis, Boca Raton

7. Verma SP, Girgis RS (1973) Resonance frequencies of electrical machine stators having encased construction, part i: Derivation of the general frequency equation. *IEEE Transactions on Power Apparatus and Systems*, PAS-92(5), pp 1577–1585
8. Girgis RS, Verma SP (1981) Method for accurate determination of resonant frequencies and vibration behaviour of stators of electrical machines. *IEEE Proc B Electr Power Appl* 128(1):1–11
9. Schwarzer M (2017) *Structural Dynamic Modeling and Simulation of Acoustic Sound Emissions of Electric Traction Motors*. Dissertation thesis, Technische Universität Darmstadt, Darmstadt
10. Gerlach ME, Bender TN, Ponick B (2022) Influence of round wire winding and insulation on the vibration behavior of electric machines. In: 2022 International Symposium on Power Electronics, Electrical Drives, Automation and Motion (SPEEDAM). *IEEE, Piscataway*, pp 7–13
11. Gerlach ME, Weber S, Ponick B (2022) Influence of hairpin winding and insulation on the vibration behavior of electric machines. In: 2022 International Conference on Electrical Machines (ICEM). *IEEE, Piscataway*, pp 635–641
12. Gerlach ME, Weber S, Ponick B (2022) Influence of concentrated winding and insulation on the vibration behavior of electric machines. In: 2022 International Conference on Electrical Machines and Systems (ICEMS). *IEEE, Piscataway*
13. Wegerhoff M, Drichel P, Back B, Schelenz R, Jacobs G (2015) Method for determination of transversely isotropic material parameters for the model of a laminated stator with windings. In: 22nd international congress on sound and vibration Florence, pp 1–8
14. Wang K, Wang X (2017) The modal analysis of the stator of the interior permanent magnet synchronous motor. In: 2017 IEEE Transportation Electrification Conference and Expo, Asia-Pacific (ITEC Asia-Pacific). *IEEE, Piscataway*, pp 1–6
15. de Barros A, Galai A, Ebrahimi A, Schwarz B (2021) Practical modal analysis of a prototyped hydrogenerator. *Vibration* 4(4):853–864
16. Mair M, Weilharther B, Rainer S, Ellermann K, Bíró O (2013) Numerical and experimental investigation of the structural characteristics of stator core stacks. *Compel* 32(5):1643–1664
17. Tang Z, Pillay P, Omekanda AM, Li C, Cetinkaya C (2004) Young's modulus for laminated machine structures with particular reference to switched reluctance motor vibrations. *IEEE Trans on Ind Applicat* 40(3):748–754
18. Allan de Barros MEG, Xang H, Langfermann M, Ponick B, Ebrahimi A (2022) Calculation of electric machines vibration using an analytical beam element model. In: 2022 International Conference on Electrical Machines (ICEM). *IEEE, Piscataway*, pp 2200–2206
19. Buntara SG (2018) *An isogeometric approach to beam structures*. Springer, Berlin Heidelberg
20. Gottstein G (2014) *Materialwissenschaft und Werkstofftechnik: Physikalische Grundlagen*, 4th edn. Springer-Lehrbuch. Springer Vieweg, Berlin
21. Gerlach ME, Ponick B (2020) Influence of the stator winding and forming of the end winding on the vibration behavior of electric machine's stator core. In: *Proceedings 2020 International Conference on Electrical Machines (ICEM)*. *IEEE, Piscataway*, pp 1171–1177
22. Gerlach ME, Zajonc M, Ponick B (2021) Mechanical stress and deformation in the rotors of a high-speed pmsm and im. *EI Elektrotech Informationstech* 138(2):96–109

**Publisher's Note** Springer Nature remains neutral with regard to jurisdictional claims in published maps and institutional affiliations.



cal design and prediction

**Martin Gerlach**, was born in Hannover, Germany, in 1992. In 2017, he graduated with a Master of Science in electrical engineering at the RWTH Aachen University. After completing his studies, he started working as a research associate at the Institute for Drive Systems and Power Electronics, Leibniz University Hannover in December 2017. His main research is in the fields of vibration and acoustics of electric machines and the mechanical design and prediction of high speed electric rotors.



His research interests relate to the computational analysis of electrical machines, including finite-element and analytic-modeling techniques.

**Allan de Barros**, was born in Osasco, Brazil, in 1992. He received the B.Sc. and M.Sc. degrees from the Polytechnic School of University of São Paulo, Brazil, in 2014 and 2019, respectively, in the field electrical engineering. He worked from 2012 to 2020 in the electromagnetic design department for hydrogenerators at Voith Hydro in Brazil. Currently, he works as a research associate at the Institute for Drive Systems and Power Electronics of Leibniz University Hannover, Germany.



**Xudong Huang**, was born in Jiangsu, China, in 1994. In 2015, he graduated with a Bachelor of Science in mechatronic engineering from Changshu Institute of Technology in Jiangsu Province, China. In 2017, he graduated with a Bachelor of Engineering from Diploma Hochschule Nordhessen, Germany, and in 2021, he completed his Master of Science in mechatronic engineering at Leibniz University Hannover.



**Markus Langfermann**, was born in Wildeshausen, Germany, in 1996. In 2022 he graduated with a Master of Science in industrial engineering from Leibniz University Hannover, where he already finished his Bachelor of Science in 2018.



**Amir Ebrahimi**, received the B.Sc. degree from Shiraz University in 2006, the M.Sc. degree in electrical engineering from the Iran University of Science and Technology in 2008, and the Ph.D. degree in electrical engineering from the University of Stuttgart, Germany. From 2013 to 2017, he was with the Fraunhofer Institute for Manufacturing Engineering and Automation, Stuttgart. Since November 2017, he has been a Professor in Electrical Machines with the

Institute for Drive Systems and Power Electronics, Leibniz University Hannover. His research interests include the analytic and numerical calculation of transient processes in electrical machines, particularly in large hydro and wind generators.



**Bernd Ponick**, was born in Großburgwedel, Germany, in 1964. He received his Dipl.-Ing. degree in electrical power engineering from the University of Hannover in 1990 and his Dr.-Ing. degree for a thesis on electrical machines in 1994. After 9 years with the Large Drives Division of Siemens as design engineer for large variable speed motors, head of electrical design and Technical Director of Siemens Dynamowerk Berlin, he is since 2003 full professor for

electrical machines and drive systems at Leibniz University Hannover. His main research activities are calculation and simulation methods for electrical machines, prediction of and measures against important parasitic effects such as magnetic noise, additional losses or bearing currents, and new applications for electric machines, e.g. for electric and hybrid vehicles or for aviation.